Thermal spin transport and spin transfer torque in ferromagnetic/non-magnetic nanoscale devices

Slachter, Abraham

Chapter 6

Spin-transfer torque and magnetization dynamics

Spin-transfer torque is defined as the torque which is exerted on a magnetization when a non-collinear spin current (i.e. where the spin direction points partially perpendicular to the magnetization) is injected into a ferromagnet[1, 2]. Here, we propose an experiment to quantify spin-transfer torque by the effect it has on the effective Gilbert damping, which determines the precession angle in ferromagnetic resonance experiments[3] and the critical switching current of spin-transfer torque magnetic memory. In a multi-terminal non-local spin valve, we measure the resistance of a precessing ferromagnet while a non-collinear spin current is injected. In order to describe spin-transfer torque in this system, we extend our commonly used 2-channel model for collinear spin transport to the more general model of non-collinear magnetoelectronics[4, 5]. We show how to construct finite-element models of spin valves which include non-collinear magnetizations. This model can be used to quantify the mixing conductance $G_{\uparrow\downarrow}$, which is a measure of spin-transfer torque. In the remainder of this chapter, we propose a novel experiment that detects the additional heat produced by a sub-micron ferromagnet in ferromagnetic resonance using an electrically isolated thermocouple.

6.1 Introduction

When a charge current flows through a ferromagnet/non-magnetic interface of a F/N/F spin valve, electron spins are injected into the non-magnetic material. These spins carry angular momentum which is absorbed by the other ferromagnet connected to the non-magnetic material[6, 7]. It was realized that the absorption of this magnetic moment, pointing in direction $\vec{s}$, can lead to a torque on the magnetization if it is perpendicular to the magnetization $\vec{M}$. This effect is known as *spin-transfer torque*[1, 2]. Using spin-transfer torque (STT), it is possible to make a tunable microwave source or

to switch the magnetic state of a ferromagnet and create a form of non-volatile magnetic memory. Both applications of spin-transfer torque were introduced in chapter 1.

In this chapter, we propose an experiment to quantify spin-transfer torque experimentally. The experiment is illustrated in Fig. 6.1. In this experiment, we use the non-local spin valve structure to inject pure spin currents (i.e. without charge currents) into a small ferromagnet. This magnet has to be small, in order to optimize the effective torque applied. The magnet is brought into ferromagnet resonance (FMR) using a static magnetic field $\vec{H}_0$ and microwave-frequency magnetic field $\vec{h}_\mu$. Ferromagnetic resonance changes the (time-averaged) resistance of the ferromagnet due to anisotropic magnetoresistance effect, which determines that the measured resistance depends on the angle between the magnetization and an applied charge current (see Fig. 6.2). By monitoring the resistance of this magnet, and scanning the magnetic field $\vec{H}_0$, it is possible to determine its resonance properties. The different shape anisotropy of both ferromagnets in the spin valve ensures they can be brought into resonance at different static magnetic fields. The magnitude and width of the resonance curves are determined by the size of the microwave magnetic field $\vec{h}_\mu$ and the ability of the magnet to damp precession: Gilbert damping. In our geometry, the direction of the applied spin-transfer torque is collinear to this Gilbert damping. By sending pure spin currents of different sign into the ferromagnet, it is possible to tune the effective Gilbert damping and therefore the resonance properties. This experiment allows to quantify the perpendicular spin current which is injected. The injected perpendicular spin current can be different from the injected collinear spin current, which is generally determined from (non-local) spin-valve measurements. A description of perpendicular spin currents in the spin valve geometry lies outside the scope of the two-channel model we have used in the previous chapters. In order to describe them, a new theory needs to be introduced which accounts for a three-dimensional spin accumulation $\vec{\mu}_s$. The interface theory as introduced by non-collinear magnetoelectronic circuit theory[4, 5] is most suitable. We show that by modeling the perpendicular spin current with finite-element methods of non-collinear spin transport, where we also use non-local spin valve signals as input, it is possible to extract the specific parameter which quantifies perpendicular spin currents: the mixing conductance $G_{\uparrow\downarrow}$ of the FM/NM interface.

When the magnet is in ferromagnetic resonance, energy is absorbed from the microwave magnetic field $\vec{h}_\mu$ to sustain the precessional motion. This heats the ferromagnet and subsequently raises the temperature. We also propose a separate experiment in which the FMR generated heat of a single sub-micron ferromagnet is detected using an on-chip thermocouple which is electrically isolated from the ferromagnet. The thermal conduction of the FMR generated heat occurs via the substrate.

The setup of this chapter is as follows. In section 6.2, we introduce the Landau-Lifshitz-Gilbert equation (LLG) which governs magnetization dynamics and include spin-transfer torque as a result of an injected spin current[1]. Next, we calculate the ferromagnetic resonance properties as a result of the applied microwave frequency and magnetic fields when a non-collinear spin current is injected. This also gives an

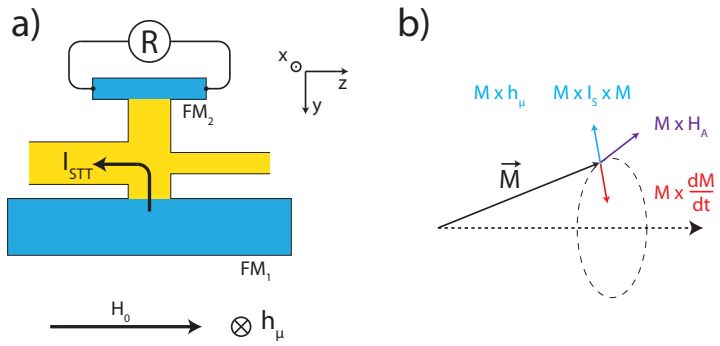

Figure 6.1: **Proposal: Spin-transfer torque tuning of the Gilbert damping detected by ferromagnetic resonance induced AMR. a)** The magnetization of FM_2 is brought into resonance by magnetic fields H_0, h_μ. The resistance of the magnet is measured while a pure spin-current is injected into FM_2 by sending a charge current I_{STT} through the non-local spin valve structure. **b)** Details of the precession process. The precession angle is determined by the balance in Gilbert damping (red), magnetization precession around the microwave magnetic field $M \times h_\mu$ and the spin-current induced torque $M \times I_s \times M$.

expression for the critical spin current which we need to inject into a ferromagnet to fully cancel the effective Gilbert damping. At this point, the magnetization fully reverses in a spin valve. This provides a criterion for the switching current in a STT-RAM device[8, 9]. In section 6.3, we introduce the concept of non-collinear magnetoelectronics and show how we can construct finite-element models of devices. We also describe the differences between this model and the diffusion model for collinear transport. In section 6.4, we calculate the heat which is generated when a ferromagnet is in resonance and propose a specific device geometry in order to measure the FMR generated heat in an experiment.

6.2 Spin-Transfer torque and magnetization dynamics

The magnetization dynamics of a ferromagnet with magnetization direction $\vec{m} = \vec{M}/M_s$ is determined by the Landau-Lifshitz-Gilbert equation (SI):

$$\frac{\partial \vec{m}}{\partial t} = -\gamma \vec{m} \times (\mu_0 \vec{H}) + \alpha \vec{m} \times \frac{\partial \vec{m}}{\partial t} - \frac{\gamma \hbar \mu_0}{2eV} \vec{m} \times \left(\vec{I}_s \times \vec{m} \right) \tag{6.1}$$

This equation has been introduced in chapter 1. In it, the gyromagnetic ratio γ determines the magnetization precession around magnetic fields. The damping of the precession is governed by the Gilbert damping parameter α and the torque exerted by a spin-current is determined by the third term. This term describes spin-transfer torque and is commonly named the Slonczewski term. The torque scales with the amount of perpendicular spin current $\vec{m} \times \left(\vec{I}_s \times \vec{m} \right)$ which is injected, but also inversely

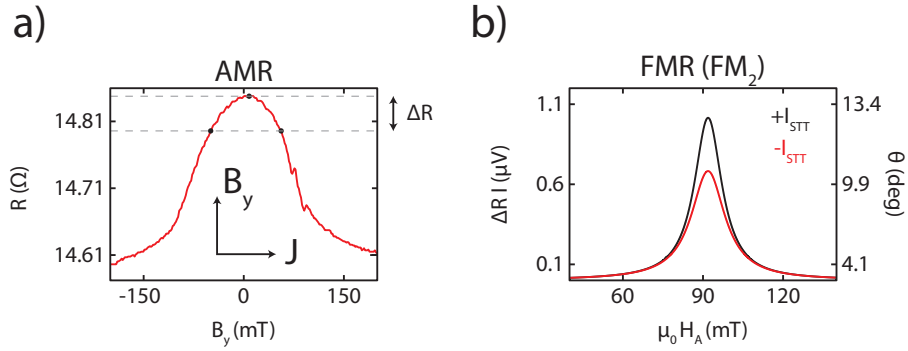

Figure 6.2: **Anisotropic magnetoresistance and calculated spin-transfer torque induced Gilbert damping. a)** Measured anisotropic magnetoresistance of a 1μm x 300 nm x 20 nm Py strip. The resistance changes as a function of the angle between the magnetization and the current. In a FMR experiment, the average precession induces a change in resistance ΔR. **b)** Calculated voltage and average precession angles observed in the FMR experiment at two different currents I_{STT}. The curves were calculated using Eqs. 6.2 and 6.9 for a magnet of 150x50x10 nm^3 with M_s = 1T, h_0 = 5mT, $\omega/2\pi$ = 12GHz, α = 0.015, ΔR = 0.2Ω and a spin current of +/- 160μA, corresponding to +/- 0.1 $I_s^{critical}$.

with the volume V of the ferromagnet. In the following we first describe how to detect FMR using the anisotropic magnetoresistance effect. Thereafter, we calculate the ferromagnetic resonance properties when a spin-torque is present.

6.2.1 AMR detection of ferromagnetic resonance

Ferromagnetic resonance is the process whereby a magnetization precession is induced around an applied magnetic field H_0 using a microwave-frequency magnetic field h_μ with angular frequency ω oriented perpendicular to H_0. The microwave magnetic field provides a torque which continuously tilts the magnetization out of its preferred axis along the applied field such that steady-state precession is achieved. This situation is sketched in Fig. 6.1. In a FMR experiment, the magnetic field $\vec{H}_0$ (or frequency) is scanned at a fixed frequency (or field) while a signal sensitive to the precession is recorded. There are several ways to record such a signal[10–13]. Recently, Costache[1] demonstrated a sensitive method which allows to detect FMR of nanoscale magnets which we will use here. It makes use of the fact that the resistance of a ferromagnet typically varies by a few percent as a function of the angle between the magnetization and the used charge current due to anisotropic magnetoresistance[2]. In a FMR measurement, the change in resistance of the ferromagnet is recorded using lock-in methods. A current I_{dc} is sent through the magnet while the amplitude of the microwave-magnetic field is modulated. A peak (or dip) in the measured signal can

[1] See chapter 6 of his thesis [3]
[2] See also section 2.2.3 of Jedema[14].

be observed when the magnetic field is scanned towards the point where the magnetization is in resonance. The resistance of the ferromagnet depends quadratically on the angle θ_{AMR} between the charge current and magnetization $R_{FM} = R_0 - \Delta R \sin^2 \theta_{AMR}$ when the angle is small. Assuming a small precession angle θ, the measured voltage V is:

$$V = I_{dc} \Delta R \theta^2 \tag{6.2}$$

Because the anisotropic magnetoresistance ΔR of the strip can be measured in a separate experiment (see Fig. 6.2a) it is possible to convert measured signals to observed precession angles. The microwave-frequency magnetic field is provided by the stray fields from microwave-frequency currents which are sent through a shorted coplanar-waveguide (CPW) or -strip (CPS) which lies nearby. The measured magnetic field position and width of the peaks as a function of frequency provides information about the intrinsic parameters of the ferromagnet. The Gilbert damping parameter α and saturation magnetization M_s can be determined, but also information about internal demagnetization and anisotropy fields is obtained. The peak height provides information about the obtained microwave magnetic field while a typically observed background can provide information about the amplitude of the microwave currents in the ferromagnet which are induced by inductive coupling to the coplanar shorts. AMR rectification experiments, in which the angle between H_0 and the easy axis is varied, also provides information about these microwave currents[3]. Often, higher order precession modes can also be observed. Studying their behavior allows to determine the behavior of non-uniform magnetization dynamics, known as spin-waves[3].

From the experimental point of view, because it is a technique which only requires two electrical contacts and a shorted coplanar waveguide/strip placed nearby ($\sim 1\mu m$), it is compatible with our standard optical/e-beam lithography process which is used to fabricate non-local spin valve devices (appendix A).

6.2.2 Spin-Transfer torque induced Gilbert damping

The ferromagnetic resonance properties of a ferromagnetic strip in the presence of spin-transfer torque is calculated by solving the LLG equation (Eq. 6.1). We consider a strip of thickness t, width w and length l where $l > w > t$ with the axis and applied magnetic fields H_0, h_μ as defined in Fig. 6.1. A static spin current I_s is injected along the direction of the applied magnetic field. In order to calculate the resonance properties, we need to consider the demagnetization field which is present $\vec{H}_d = -\bar{N} \cdot \vec{M}$, where $\bar{N}$ is the demagnetization tensor. For simplicity, we approximate our brick shaped magnet by an ellipsoid of similar dimension such that this tensor is diagonal and can be explicitly calculated[16]. We further assume $l \gg t, w$ such that N_z=0. Due to the large demagnetization field in the thickness direction, the precession is elliptical. The precession angle is larger in the width direction then in the thickness direc-

[3]For example, see chapter 6 of Sladkov[15]

tion. The average precession angle θ obtained in experiments is generally small, such that we can search for a steady state solution $\vec{M}(t) = \left(m_x e^{j\omega t}, m_y e^{j\omega t}, M_s\right)$ as a result of a microwave-frequency magnetic field $h_\mu = h_0 e^{j\omega t}$ of angular frequency ω. The effective magnetic field inside the strip is then $\vec{H} = \left(h_0 e^{j\omega t} - N_x m_x e^{j\omega t}, -N_y m_y e^{j\omega t}, H_0\right)$. Neglecting terms higher then linear in α, we obtain the equations of motion in the presence of a spin transfer torque:

$$(j\omega + \beta)\, m_x = -\left(\gamma H_0 + N_y M_s + j\omega\alpha\right) m_y \tag{6.3}$$

$$(j\omega + \beta)\, m_y = (\gamma H_0 + N_x M_s + j\omega\alpha)\, m_x - \gamma M_s h_0 \tag{6.4}$$

Where we have defined a spin-transfer torque coefficient $\beta = \gamma\hbar\mu_0 I_s / (2eVM_s)$. Setting h_0=0, and ignoring all terms α, β except a β^2 term, the above equations can be solved to obtain the resonance condition:

$$\omega_0^2 = \gamma^2 (H_0 + N_x M_s)\left(H_0 + N_y M_s\right) + \beta^2 \tag{6.5}$$

This is the Kittel formula for ferromagnetic resonance[17] with an alteration due to spin-transfer torque. In practice, the alteration is very small and can be ignored. We keep it here for further notational simplicity. It is convenient to describe the solutions in terms of complex susceptibilities χ_L, χ_T such that $m_x = \chi_L h_0$, $m_y = \chi_T h_0$. They determine the amplitude and phase of the precession of both directions. The amplitude is generally much larger then h_0. The solutions are:

$$\chi_T = \gamma M_s \frac{\beta + j\omega}{\omega^2 - \omega_0^2 - j\omega A} \tag{6.6}$$

$$\chi_L = -\gamma M_s \frac{\gamma H_0 + j\omega\alpha}{\omega^2 - \omega_0^2 - j\omega A} \tag{6.7}$$

Where we have defined an effective damping parameter A= $\alpha\gamma\,(2H_0 + M_s) + 2\beta$. From these results, all the resonance properties can be determined such as for example the phase of the precession $\arg(\chi_L)$, $\arg(\chi_T)$ or the ellipticity $\epsilon = |\chi_L/\chi_T|$. Of particular interest is the time-averaged precession angle $\theta = \frac{1}{2M_s}\left|m_x + m_y\right|_{t-avg}$ at the resonance condition ω=ω_0. Under the usual conditions H_0<M_s and assuming spin-transfer torque is relatively small we obtain the simple expression $\theta = h_0/2\alpha' M_s$, where we have defined an effective Gilbert damping parameter α':

$$\alpha' = \alpha + \frac{\hbar\mu_0}{eM_s\,(2H_0 + M_s)} \frac{I_s}{V} \tag{6.8}$$

Using spin-transfer torque, it is possible to tune the effective Gilbert damping parameter α' which determines the precession angle and also the width of the resonance peaks. In our electrical detection scheme, the observed signals are sensitive to θ^2. The

time-averaged square angle is given by $\theta^2|_{t-avg} = h_0^2(|\chi_L|^2 + |\chi_T|^2)/2M_s^2$. Evaluating it gives:

$$\theta^2|_{t-avg} = \frac{1}{2}\gamma^2 h_0^2 \frac{(\gamma H_0)^2 + \beta^2 + \omega^2(1+\alpha)}{(\omega^2 - \omega_0^2)^2 + (\omega A)^2} \tag{6.9}$$

This formula can be used to fit the measured results in a ferromagnetic resonance experiment. The fit strategy as used by Costache[3] allows an accurate determination of M_s, $\bar{N}$, $h_0(\omega)$ and α. Various strategies can be used to determine the injected spin-current I_s from experiments. For example, we may fit Eq. 6.9 at fixed frequency for different charge currents I_{dc} used for spin-injection with a single fit parameter ν determining the spin current $I_s = \nu I_c$. If we vary the precession angle by varying the applied microwave-frequency magnetic field h_0, this will allow us to determine ν as a function of the average precession angle θ. An calculated example of a FMR induced AMR resistance is given in Fig. 6.2, where the observed voltage is shown for a small 150x50x10 nm^3 ferromagnet at two different spin currents.

6.2.3 Spin-transfer torque switching

In the previous section we have observed that the effective Gilbert damping can be tuned by injecting a spin current in ferromagnetic resonance experiments. Eq. 6.5 shows that even in the absence of an applied magnetic field H_0 it is possible to obtain a resonance condition. In this case, the magnetization precesses around its own demagnetization field. The ferromagnetic resonance angle is determined by the balance between Gilbert-damping, the torque exerted by precession around the magnetic field h_μ and spin-transfer torque (see Fig. 6.1b). Whenever spin-transfer torque is strong enough, it is possible to fully cancel the effective Gilbert damping or even reverse it. In this case, no magnetic field h_μ is needed to induce a precessional motion. Any instantaneous, for example thermally excited, off-axis magnetization will result in a precessional motion which is amplified. This amplification stops when the precession angle becomes larger then 90 degrees. The effective Gilbert damping then reverses and the precession is strongly damped. This process is known as *spin-transfer torque switching*. It was introduced before in chapter 1, where the magnetization reversal process was illustrated in Fig. 1.3b. A minimal requirement for the spin current is given by the effective Gilbert damping, which should be negative. We define a critical spin current $I_s^{critical}$ at which the precessional damping is canceled (α'=0) and spin-transfer torque switching becomes possible[9]:

$$\frac{I_s^{critical}}{V} = \frac{\alpha e M_s(2H_0 + M_s)}{\mu_0 \hbar} \tag{6.10}$$

Under certain conditions, usually just before the actual the actual spin-transfer torque switching, it becomes possible that the precession is initially amplified but becomes stable at a precession angle <90 degrees. In this case, magnetization dynamics is induced using a static spin-current; a concept known as the spin-torque oscillator[18–22]. The magnetization reversal time of spin-transfer torque switching depends on

the actual applied spin-torque I_s. We illustrate this by a small numerical calculation. For the magnet considered in Fig. 6.2 we can calculate this numerically by solving the LLG equation[4]. We find a switching time of ~140 ns at $I_s = I_s^{critical}$ which quickly drops of to ~5 ns at $I_s = 2I_s^{critical}$ for an initial magnetization of $\vec{m} \approx (10^{-4}, 0, 1)$. This example illustrates the typical timescales for spin-transfer torque switching and is the limiting factor in the writing speed of STT-RAM devices.

6.3 Non-collinear magnetoelectronics

Spin-transfer torque is determined by the perpendicular component of the spin current ($\vec{s} \perp \vec{m}$) which is injected into a ferromagnet. This spin current can be different from the spin current in the collinear case ($\vec{s} \parallel \vec{m}$), which is usually determined by fitting the results from a (non-local) spin valve experiment to a model of spin-transport. The 2-channel model introduced in chapter 1 accurately describes spin-transport in (non-local) spin-valves and is often used because of its simplicity[7, 23–26]. The spin valve signals, also determining the spin currents, are fitted by a single parameter P_I[5], the spin polarization of charge transport in the bulk ferromagnet. In order to describe non-collinear spin currents, we introduce a new theory which is named the non-collinear magnetoelectronic circuit theory[4, 5][6]. In it, the spin accumulation becomes a three-dimensional vector $\vec{\mu}_s$. We can model our devices by constructing finite-element models of this theory. This theory is fundamentally different from the previously considered 2-channel model. As opposed to the 2-channel model which is determined by *bulk* properties, spin injection in this theory is determined by the quantum mechanical scattering properties of the ferromagnetic/non-magnetic *interface*. In this theory, there are different interfacial conductivities $G_\uparrow$, $G_\downarrow$ for spin species parallel or antiparallel to the magnetization. The perpendicular spin currents through the F/N interface are determined by a separate entity, the mixing conductance $\vec{I}_{s,\perp} \sim G_{\uparrow\downarrow}\vec{\mu}_{s,\perp}$. It is a flexible theory preferred by theorists, because the parameters can be fully determined from quantum-mechanical transmission and reflection coefficients of spin populations and can be calculated ab-initio. In this theory, it is also trivial to include tunnel junctions which makes it very general. The mixing conductance represents the non-spin preserving quantum-mechanical reflection of a perpendicular spin population coming from the non-magnetic side. This effect determines the torque on

[4] This calculation is generally simplified by replacing $\vec{m} \times \frac{d\vec{m}}{dt}$ by $\vec{m} \times (-\gamma\vec{m} \times \vec{H})$ and calculating the change in magnetization $\Delta\vec{m}$ as a function of time steps Δt. This is an approximation which is accurate for the underdamped system we consider($\gamma\vec{m} \times \vec{H} \gg \alpha\vec{m} \times \frac{d\vec{m}}{dt}$). See also Sun[9]

[5] Perhaps more often $P_I\lambda_F$ is used as the fit parameter, because the ferromagnetic relaxation length λ_F is not always known from experiments.

[6] We note that it is also possible to extend the 2-channel diffusion model to a diffusion model which includes a spin-independent potential $\mu_c = (\mu_\uparrow + \mu_\downarrow)/2$ and three-dimensional spin potential $\vec{\mu}_s$ which are still continuous variables over interfaces. In this case, spin relaxation is governed by the Valet-Fert equation $\nabla^2\vec{\mu}_s = \vec{\mu}_s/\lambda$. In order to describe non-collinearity, the ferromagnet relaxation length can be made anisotropic, similar to our previous description of anisotropic magnetoresistance (Eq. 5.3). However, this is not a realistic description, since in the ferromagnet the non-collinear precession length is smaller then the mean free path[4, 5].

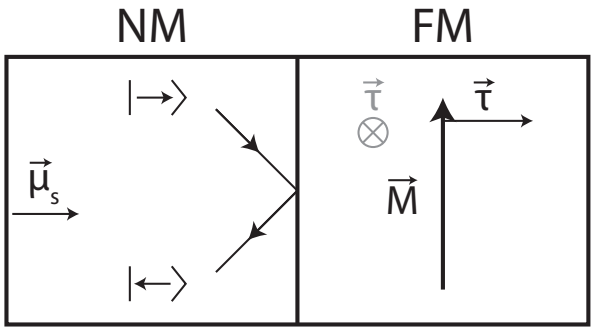

Figure 6.3: **Schematic of spin-transfer torque.** A perpendicular spin population $|\rightarrow\rangle$ approaching the ferromagnet fully reflects of the interface. The reflection is full because perpendicular spins strongly dephase in the ferromagnet due to internal magnetic fields such that a stable population $|\rightarrow\rangle$ is not possible in the ferromagnet. The non-spin-conserving reflections cause a transfer of angular momentum to the magnetization known as spin-transfer torque. The resulting perpendicular spin current $\vec{J}_s^{\perp}$ is determined by the spin accumulation $\vec{\mu}_s$ in the non-magnetic material and the complex mixing conductance $G_{\uparrow\downarrow}$. There exists a small probability that the reflecting spin population effectively rotates along the strong internal magnetic field of the ferromagnet leading to transfer torque $\sim \vec{\mu}_s \times \vec{m}$. In general, $\mathrm{Re}(G_{\uparrow\downarrow}) \gg \mathrm{Im}(G_{\uparrow\downarrow})$ and therefore this term is commonly ignored.

the magnetization, and is explained in Fig. 6.3.

6.3.1 Theory

A thorough introduction into magnetoelectronic circuit theory is given by Brataas[4]. Here, we will describe how to apply this theory and construct finite-element models of devices which can be used to fit parameters from this theory. In non-collinear magnetoelectronics, bulk diffusion of the charge μ_c and three-dimensional spin-accumulation $\vec{\mu}_s$ is determined by charge and spin current continuity in the non-magnetic material. This continuity results in the Poisson $\nabla^2\mu_c = 0$ and Valet-Fert equation $\nabla^2\vec{\mu}_s = \vec{\mu}_s/\lambda^2$ in the bulk non-magnetic material. It is essentially identical to a generalized version of the 2-channel model.

In a ferromagnet, any perpendicular spin population needs to be decomposed in the two eigenstates of the magnet($|\rightarrow\rangle = |\uparrow\rangle \pm |\downarrow\rangle$), which point parallel and antiparallel to the magnetization. The quantum-mechanical oscillation frequency of both spin components is determined by the wave vectors $k_F^{\uparrow}, k_F^{\downarrow}$ of these states. The energy splitting of the bands in a ferromagnet is generally so large, that the distance at which such a spin population dephases, the ferromagnetic coherence length $\pi/|\lambda_F^{\uparrow} - \lambda_F^{\uparrow}|$, is in the order of the atomic spacing. This is much smaller then the mean free path,

which makes it impossible to speak of a stable perpendicular spin population in the ferromagnet. In non-collinear magnetoelectronics, the spin-dependent transport is determined by the properties of the interface. Since collinear spins are generally also very short lived in ferromagnets[7], we will use the often implied assumption to ignore spin-accumulations altogether in the ferromagnet. This has the added advantage of reducing the amount of free parameters in this model. In the bulk of the ferromagnet, we only need to describe the chemical potential, which is determined by the Poisson equation $\nabla^2\mu_c = 0$. Spin injection and detection is determined by the boundary conditions at the F/N interface, which relate the charge- and spin-accumulation to the charge and spin currents. In non-collinear magnetoeletronics, these are written in terms of 2x2 density matrices[8]:

$$\bar{\mu} = \mu_c \bar{1}_2 + \bar{\sigma} \cdot \vec{\mu}_s \tag{6.11}$$

$$\bar{J} = J_c \bar{1}_2 + \bar{\sigma} \cdot \vec{J}_s \tag{6.12}$$

Where $\bar{\sigma}$ are the 2x2 Pauli spin-matrices and I_2 the 2x2 identity matrix. Charge and spin transport through the interface is then determined by a 2x2 conductance matrix $\bar{G}$:

$$\bar{J} = \bar{G}\left(\bar{\mu^N} - \bar{\mu^F}\right) \tag{6.13}$$

$$\bar{G} = \begin{pmatrix} G_\uparrow & G_{\uparrow\downarrow} \\ G^*_{\uparrow\downarrow} & G_\downarrow \end{pmatrix} \tag{6.14}$$

In our model, a spin-accumulation does not exist in the ferromagnet. However, non-spin preserving reflection can still transfer angular momentum to the ferromagnet, which results in effective spin-currents at the interface. In this model, the 5 parameters $\mu_c^F, \mu_c^N, \vec{\mu}_s$ and their corresponding currents are determined through charge current continuity and Eq. 6.13. It is intuitive to decompose Eq. 6.13 into parallel and perpendicular spin currents. Collinear spin- and charge-transport is then determined by:

$$J_c = G\left(\mu_c^N - \mu_c^F\right) + PG\vec{\mu}_s \cdot \vec{m} \tag{6.15}$$

$$\vec{J}_s^{\parallel} = \left(PG\left(\mu_c^N - \mu_c^F\right) + G\vec{\mu}_s \cdot \vec{m}\right)\vec{m} \tag{6.16}$$

Where we have defined an overall interface conductance $G = G_\uparrow + G_\downarrow$ and interface polarization $P = (G_\uparrow - G_\downarrow)/(G_\uparrow + G_\downarrow)$. Unlike the 2-channel model, which has a single fit parameter, two parameters P, G are present to model spin and charge transport in

[7] Generally for metals, the spin-diffusion length is slightly larger, or even in the order of, the mean-free path making a diffusive description only just valid for transparent contacts[14].

[8] For an introduction, see also chapter 3, E_{III} of [27]

devices. The perpendicular spin current consists of two components, related to the real and imaginary part of the mixing conductance $G_{\uparrow\downarrow}$:

$$\vec{J}_s^{\perp} = 2Re(G_{\uparrow\downarrow})\vec{m} \times (\vec{\mu}_s \times \vec{m}) + Im(G_{\uparrow\downarrow})\vec{\mu}_s \times \vec{m} \tag{6.17}$$

We ignore the imaginary part of the mixing conductance, because it is generally very small[28]. In order to interpret how these equations govern spin transport, we consider two simple examples. First, consider a charge current flowing through the F/N interface. Eq. 6.15 shows a potential $\mu_c^N - \mu_c^F$ develops across the interface, even at P=0. In the presence of an interface conductance P, this potential induces a finite spin-current (Eq. 6.16) which causes a spin accumulation to occur in the non-magnetic material pointing (anti-)parallel to the magnetization. This illustrates the concept of spin-injection. Also, when a parallel spin accumulation is provided by an external source to this interface, Eq. 6.15 shows a interface potential must build up in the absence of charge currents if the interface polarization is non-zero. This describes spin detection. The two processes combined describe collinear spin transport in a (non-local) spin valve device. Whenever a perpendicular spin accumulation is present at the F/N interface, this situation is different. If the mixing conductance is zero, the interface is fully isolating $\vec{J}_s^{\perp} = 0$ (Eq. 6.17), but in all other cases a perpendicular spin currents will be drawn from the source of perpendicular spin accumulation. In other words, collinear spin transport is governed by the interface polarization and conductance P, G and perpendicular spin transport is determined by the mixing conductance $G_{\uparrow\downarrow}$.

The difference between collinear and perpendicular spin transport is largest when we consider tunnel contacts. In this case $G \to 0$, and no collinear spin currents will occur as a response to a parallel spin accumulation which is present. The ferromagnetic contact acts as a 'perfect' probe because there is a spin-dependent potential drop $\mu_c^F - \mu_c^N = P\mu_s$ but no spin current. However, the mixing conductance depends on non-spin preserving reflection of states at the interface and is generally not much reduced when going from transparent contacts to tunnel contacts. By tuning the angle between the magnetization and the spin current, it is possible to tune the absolute spin current which is drawn by the magnet. This property of tunnel interfaces makes spin-transfer torque very efficient. An efficiency η can be defined by the spin current drawn from parallel and perpendicular spin accumulations η=2Re($G_{\uparrow\downarrow}$)/($G_\uparrow + G_\downarrow$). Xia[28] has calculated the conductances for the Co/Cu and Cr/Fe interface with and without tunnel contacts. For transparent contacts, $\eta \approx 1.5 - 2$ while for tunnel contacts it can be up to 10^{10}. This illustrates the increased efficiency when tunnel contacts are used.

In our experiment, we use transparent F/N contacts in the non-local spin valve geometry and use small precession angles. In this case, the perpendicular spin current should scale ~linearly with the angle, such that the theory applied in section 6.2 is valid. In the following, we propose the fabrication of an optimized Py/Cu/Py non-local spin valve device. We show how we can relate the various measured quantities to the P, G and $G_{\uparrow\downarrow}$ parameters of the model.

6.3.2 Proposed device

In order to demonstrate spin-transfer torque tuning of the Gilbert damping in a non-local spin valve device, we need to consider a device in which the dimensions are optimized such that the pure spin-current which is injected into a ferromagnet is largest. At the same time, the ferromagnet needs to be small because the applied spin-transfer torque scales inversely with the volume. Finally, at least four contacts need to be present in order to probe the 4-contact resistance of the ferromagnet. Here, we propose an optimized device which can be fabricated using our standard fabrication technique (appendix A) and allows to measure the effect we propose. The device and a finite-element model calculation are shown in Fig. 6.4.

The device consists of two Permalloy ($Ni_{80}Fe_{20}$) ferromagnets of 1000x300x25nm^3 (FM_1) and 160x40x10 nm^3 (FM_2) size which are connected by a 60 nm thick Copper 'fork' (contacts 1,4) and several 30 nm thick gold contacts (contacts 2,3,5). A spin current is injected into FM_2 by sending a charge current I_{1-2}. The non-local spin valve signal is measured by probing the voltage V_{4-5} and scanning the collinear magnetic field H_0. This allows to obtain information about the size of the collinear spin-currents, as we will show next. The resistance of FM_2 is measured by sending an additional (smaller) dc charge current I^{dc}_{1-3} and probing V_{4-5} such that a ferromagnetic resonance experiment can be performed. The two current sources which are used for spin-injection and FMR-detection share a common ground in this geometry.

We construct a finite-element model of the device using both the 2-channel model and a model which uses non-collinear magnetoelectronic circuit theory (the non-collinear model). The 2-channel model has one input parameter (P_I) to fit measured spin-valve signals while the non-collinear model has two (G, P). In order to overcome this complication, we introduce an additional constraint. The background resistance measured in the non-local theory is often thermoelectric in nature. However, when the ferromagnets are very close to each other, the 2-channel model also provides a good description of the measured non-thermoelectric background[29]. We use the calculated background of the 2-channel model as input for the non-collinear model. The non-local background resistance varies only slightly when the interface resistance is varied (see Fig. 6.4b). We find that the background resistance of both models correspond whenever the interface resistance 1/G is equal to the ferromagnetic spin-resistance R_F in the 2-channel model. We use this value in our following calculations.

In the non-local spin valve measurement, the spin-valve signal can be fitted to the interface polarization P. Fig. 6.4c shows a calculated spin-valve signal versus the interface polarization, which has a quadratic dependence. For the parameters used in chapter 3, we can calculate a non-local spin valve signal of $\approx 5.5 m\Omega$ for this device using the 2-channel model. This corresponds to the calculated non-local spin valve signal in the non-collinear model when the interface polarization $P = 0.3$ which we use in the following. In the non-collinear model, we now only have one parameter left to quantify from experiment; the mixing conductance $G_{\uparrow\downarrow}$. This parameter can be quantified by determining the perpendicular spin currents from ferromagnet resonance experiments where the angle and width of the resonance curves are tuned by

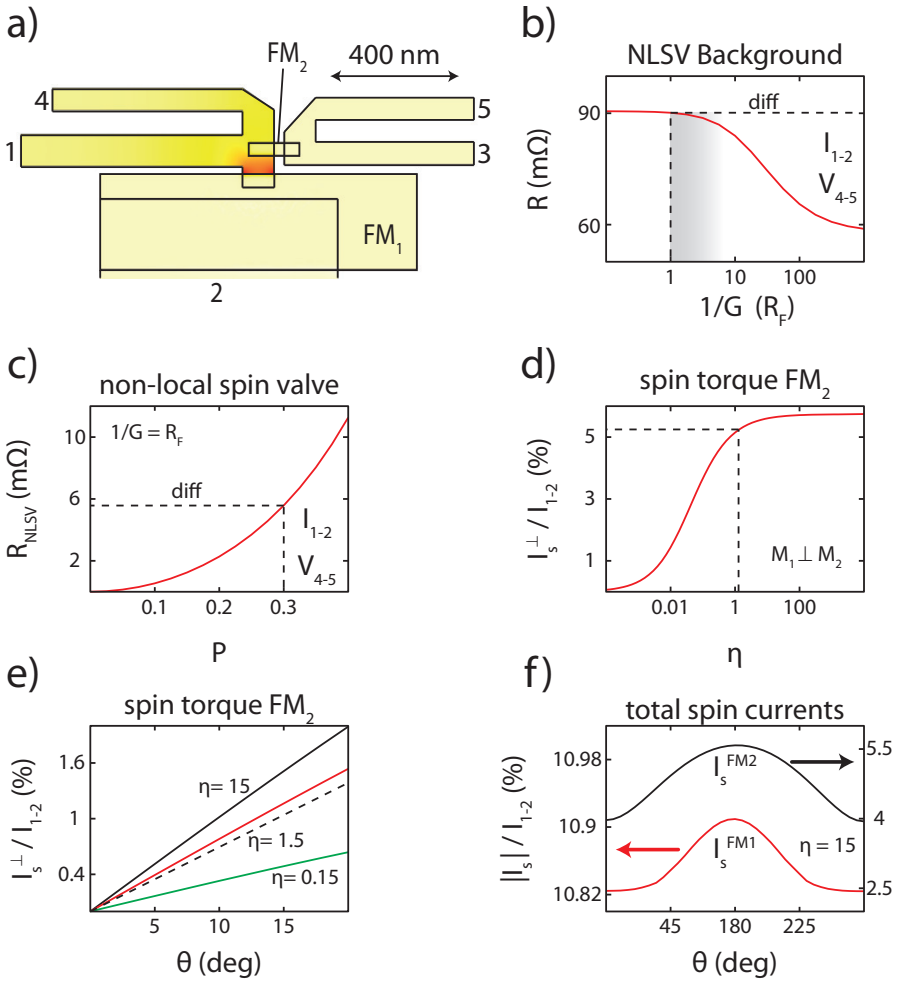

Figure 6.4: **Proposed device to study STT-induced Gilbert damping and calculation. a)** Proposed non-local spin valve geometry with plotted spin-accumulation (a.u.), calculated from non-collinear magnetoelectronic circuit theory. **b)** The calculated background resistance in a non-local spin valve measurement as a function of the interface conductance G. **c)** The spin-valve signal as a function of the interface spin-polarization. **d)** Spin-transfer torque current $I_s^{\perp}$ as a function of the mixing conductance η=2Re$G_{\uparrow\downarrow}/G$ when the two magnetizations are oriented perpendicular. **e)** Spin-transfer torque current as a function of the angle θ between the magnetizations. **f)** The total spin current which flows through the F/N interface as function of θ. Dashed lines indicate the results from the 2-channel model and expected η=1.5[28] for transparent interfaces.

spin-transfer torque. Fig. 6.4d shows a calculation of the perpendicular spin current as a function of the mixing conductance η=2Re$G_{\uparrow\downarrow}/G$ when the magnetizations are perpendicular. It shows that the perpendicular spin current slightly varies as function of the mixing conductance. A calculation of Xia[28] shows that for transparent Co/Cu contacts, the mixing conductance $\eta \approx 1.5$. This is indicated in the figure by the dashed line. At this moment, the perpendicular spin current is about 5% of the charge current sent through the device.

In our calculation, we implicitly assumed that the injected perpendicular spin-current in a ferromagnetic resonance experiment $I_s^{\perp} = \vec{m} \times \vec{I}_s^{\parallel} \times \vec{m}$ scales with the injected component of the spin current. Fig. 6.4e shows a calculation of the perpendicular spin current at small magnetization angles for various magnitudes of the mixing conductance. We observe that it scales linearly with the magnetization angle and that the dependence on η is weak. It is approximately equal to a prediction from the parallel current in the collinear case, justifying the assumption we used. Fig. 6.4f shows that even for a fairly large mixing conductance, the spin current which is emitted by FM_1 is around 10% of the charge current, and is hardly influenced by the magnetization angle. However, the total amount of spin current which is injected into FM_2 increases due to to large mixing conductance. It illustrates that the injection and detection of spins is largely decoupled in a non-local spin valve device.

Using the expected parameters $1/G = R_F$, P=0.3 and $\eta = 1.5$, we calculate how much the Gilbert damping can be tuned in ferromagnetic resonance experiments on this device, and what signals we expect. Using the dimensions of FM_2, we calculate the critical switching spin-current (Eq. 6.10) to be I_s^{crit}=1.2 mA[9]. A fit on the obtained perpendicular spin current at small angles (Fig. 6.4e) shows that the effective parallel spin current used in the FMR modeling of spin-transfer torque is 4.4% of the charge current. Device failure is limited by electromigration, which determines the maximum charge current density ($J \approx 10^{12}$ A/m^2) which can be sent through the device. From the modeling, we see that we can send a maximum current of 4 mA through the device which corresponds to a maximum parallel spin-current of 170 μA. Using this information, we deduce that the effective Gilbert damping can be tuned by a maximum of ≈15%.

The 4-point resistance of FM_2 is 27Ω, which includes a 4Ω contact resistance. We have calculated the spin-transfer torque tuning of FMR in Fig. 6.2 which assumed very similar parameters. This shows the proposed geometry is very reasonable to demonstrate spin-transfer torque induced Gilbert damping. We note that the non-collinear model used here can also be applied to lateral spin valves which include tunnel contacts with an increased efficiency. We use the analysis developed here to study the experimental results on spin-transfer torque tuning of the Gilbert damping in chapter 7.

[9] In this calculation, we used M_s=1T, α=0.15 and the demagnetization tensor calculated by 6.22, 6.23

6.4 On-chip thermal detection of ferromagnetic resonance

When the magnetization of a ferromagnet is brought into resonance, it absorbs energy from the magnetic field to sustain the precessional motion. The continuous absorption of energy raises the temperature of the ferromagnet. In this section, we calculate this heating, and propose the aimed detection of the generated heat from a nanoscale ferromagnet by placing a thermocouple nearby. Because thermal conduction of heat also occurs via the substrate, this thermocouple does not have to be electrically connected to the ferromagnet. In theory, this measurement technique allows to detect ferromagnetic resonance of even smaller ferromagnets then in the electrical detection scheme of Costache[3], because it does not require multiple electrical contacts. In the following, we first calculate the magnetic energy which is absorbed by a ferromagnet when it is in resonance. Next, we calculate two examples using the thermoelectric finite-element model[10].

Energy absorption in FMR

We have calculated the ferromagnetic resonance properties of a single domain ferromagnet in section 6.2 by solving the LLG-equation. As sketched in Fig. 6.1, ferromagnetic resonance occurs because the Gilbert damping is canceled by precession of the magnetization around the microwave-frequency magnetic field h_μ. The power which is dissipated when the magnetization is in resonance can be calculated from the magnetic energy E in the magnet:

$$E = \mu_0(\vec{M} \cdot \vec{H}) \tag{6.18}$$

The power which needs to be drawn from the magnetic field in order to stabilize the precessional motion in ferromagnetic resonance is equal to the rate of change in magnetic energy dE/dt if there is no microwave magnetic field. For simplicity, we first consider a ferromagnet whose short axis are equal $t{=}w \gg l$. In this case, the precession is such that we can consider the cross section of the magnetization and the easy axis, depicted in Fig. 6.5a. The rate of change in magnetization which changes the magnetic energy is determined by the Gilbert damping. Note that the precessional motion $\gamma M \times H$ does not influence the magnetic energy. We assume the magnetization precesses with angle θ and angular frequency ω around the magnetic field H_0. The frequency is determined by the Kittel formula (Eq. 6.5). The Gilbert damping $\vec{G} = \alpha\vec{m} \times d\vec{m}/dt$ (s^{-1}) tilts the magnetization towards the easy axis. This changes the the magnetic energy contribution due to the static magnetic field $M \cdot H_0$, but also that due to the demagnetization field $M \cdot H_d$. The demagnetization field $H_d = -N_\perp M_z$ is determined by the magnetization component in the $\hat{z}$ direction and the perpendicular demagnetization coefficient $N_\perp$. We consider an ellipsoid shape for

[10] See chapters 2-5 or Bakker[29].

the ferromagnet, in which case $N_\perp \approx 0.5$. We assume that the Gilbert damping is relatively small, such that we have an underdamped system. In this case, the largest portion of dm/dt in the LLG equation is that due to precession $dm/dt = \omega M_s \hat{y}$. Using this expression in the Gilbert damping G, it is now straightforward to calculate the dissipative power $P = dE/dt$ of Gilbert damping:

$$P = \alpha\omega\mu_0(H_0 + 2N_\perp M_s)M_s\theta^2 \tag{6.19}$$

This power is the generated heat of a ferromagnet in resonance. It intuitively scales with the Gilbert damping, frequency, the saturation magnetization and applied magnetic field. In a typical experiment, the short axes t, w are not equal, and we need to consider elliptical precession. Therefore, we generalize the obtained result. In case of an elliptical precession, the precession occurs on one axis with angle θ_1 and demagnetization factor N_1 and on the other axis with angle θ_2 and demagnetization factor N_2. The ellipticity is defined as $\epsilon = \theta_2/\theta_1 < 1$. By the symmetry of the problem, the angle $\theta^2(t) = \theta_A^2 + \Delta\theta^2 \sin(2\omega t)$ and effective perpendicular demagnetization factor $N_\perp(t) = N_A + \Delta N \sin(2\omega t)$ have time-independent terms and time-dependent terms which oscillate with frequency 2ω. Here we have defined an average squared angle θ_A^2 and demagnetization factor N_A and their differences $\Delta\theta^2, \Delta N$. We are only interested in the time-independent term in the power P(t). After a small calculation, we obtain:

$$P|_{t-avg} = \alpha\omega\mu_0(H_0 + 2\eta M_s)M_s\theta^2|_{t-avg} \tag{6.20}$$

Where there is an effective factor η which depends on the ellipticity of the precession:

$$\eta = N_A - \frac{1}{2}\Delta N\frac{1-\epsilon^2}{1+\epsilon^2} \tag{6.21}$$

The ellipticity is given by $\epsilon = |\chi_L/\chi_T|$, and can be calculated from Eqs. 6.6 and 6.7 while the time averaged precession angle $\theta^2|_{t-avg}$ is given by Eq. 6.9. The demagnetization factors can be estimated from those of a spheroid[16], which we will give here for completeness:

$$N_t = \frac{2}{\pi}\arctan\left(\frac{w}{t}\frac{l}{L'}\right) \tag{6.22}$$

$$N_w = \frac{2}{\pi}\arctan\left(\frac{t}{w}\frac{l}{L'}\right) \tag{6.23}$$

Where $L' = \sqrt{l^2 + w^2 + t^2}$ and $N_l = 1 - N_t - N_w$. In a typical experiment $M_s > H_0$ and $t < w \ll l$ and we have a small ellipticity in which case we can obtain the simple expression $\eta \approx t/w$. We see that in order to maximize the dissipated heat, we need a square ($w = t$) magnet[11]. We may use thermoelectric finite-element modeling to calculate the actual heating of a ferromagnet, which is in general thermally connected to

[11] We note that in addition, the eigenfrequency of a square magnet is optimized in this case.

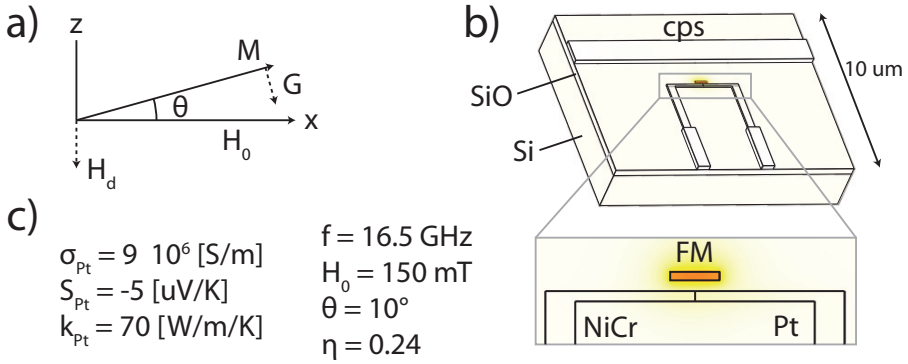

Figure 6.5: **Thermal detection of ferromagnetic resonance of a nanoscale magnet. a)** Details of the calculation. **b)** Example of a possible experiment which measures ferromagnetic resonance heating of a 500x80x30nm^3 Permalloy ferromagnet using a NiCr-Pt thermocouple which is electrically isolated and thermally connected to a ferromagnet. The NiCr-Pt thermocouple is positioned 100 nm away from the ferromagnet. A signal of ΔV=140 nV is expected to occur at the thermocouple for the resonance parameters indicated in **c)**. When the magnet is embedded into the thermocouple (not shown), this signal increases to 480 nV.

the environment via the substrate and possible contacts. Such a model has been used in chapters 2-5. In it, we can use the time-averaged power to calculate FMR heating and the associated voltages. In order to do this, the equation for the continuity of the heat currents is altered for the ferromagnet: $\Delta Q = J^2/\sigma + P|_{t-avg}$. In the following, we calculate an example in which we detect the heat with an on-chip thermocouple.

Thermal detection using thermocouples

The generated heat of a ferromagnet of which the magnetization is brought into resonance can be detected by a variety of means. For example, we may monitor the resistance of a nearby piece of material which depends on the temperature of this material[30]. In chapters 2-5 we have shown that using lock-in techniques, an on-chip thermocouple can be very sensitive in detecting induced temperature differences[12]. As an example, we calculate the thermoelectric voltage of a NiCr-Pt thermocouple ($\Delta S \approx 25\mu V/K$) due to the heat generated from a 500x80x30 nm^3 Permalloy ferromagnet. The geometry is depicted in Fig. 6.5b. A $1\mu m$ wide short of a coplanar waveguide/strip lies nearby to deliver large microwave frequency currents which generates the necessary microwave-frequency magnetic field. Near the maximum power of a typical microwave source $P = 20dBm$, a charge current of 45 mA flows through the short of a coplanar strip, which generates a microwave frequency magnetic field of 6 mT. For the typical Py parameters $\alpha \approx 0.015$, M_s=1T we obtain precession angles of $h_\mu/2/\alpha M_s$=10 degrees.

[12] See for example Fig. 4.5 in which the temperature resolution ~ $100\mu K$ for a NiCr-Py thermocouple

The substrate plays a crucial role in the detection of the heat. In microwave experiments, usually an i-Si substrate of high purity ($\rho > 10^3 \Omega cm^{-2}$) is used. Such a substrate has nearly metallic thermal conductivity, which severely limits the heating of the ferromagnet. Therefore, we use a substrate which has a 300 nm (thermally grown) oxide that has a much lower thermal conductivity[13]. Using the typical resonance parameters for this ferromagnet in Fig. 6.5c, we calculate that the ferromagnet heats up by 20 mK which generates a thermoelectric voltage of $V_{NiCr-Pt}$=140 nV. This is above the noise limit in an experiment which modulates the microwave frequency (a few nV). When we embed the magnet in the center of the thermocouple, this voltage increases to 480 nV due to the improved thermal conductance. The modeling also allows us to determine other parameters in the experiment, such as the heating of the coplanar short and the resulting thermoelectric background voltage. Due to the small thermally conductivity of the Siliconoxide, the short heats up ~100 degrees which generates thermoelectric background voltages of ~1mV. This is a large but not uncommon background voltage. Double modulation techniques have been developed to overcome the additional noise which is generated by this[3]. In theory, the heating can be prevented by growing a selective oxide under the ferromagnet and thermocouple but not under the coplanar short. A calculation on a separate finite-element model shows this reduces the background-heating and -voltage by a factor 10. From AMR-rectification experiments, it is known that microwave currents of ~0.1% of the microwave current through the short are induced in our thermocouple. They are induced due to inductive coupling of the measurement loop to the coplanar waveguide and will generate a background of 500 nV at a typical induced microwave current of 10μA. This example shows it is possible to construct an experiment which detects the heat from a ferromagnet brought into ferromagnet resonance using an on-chip thermocouple.

6.5 Conclusion & Outlook

In this chapter, we have calculated the resonance properties of a ferromagnet under the influence of spin-transfer torque. We have introduced the theory of non-collinear magnetoelectronics[4] in order to describe the magnitude of the spin-currents which are responsible for spin-transfer torque in spin valve devices. Using this theory, we have proposed an experiment which quantifies the perpendicular spin currents in a non-local spin valve geometry by the spin-transfer torque which is exerted on the ferromagnetic resonance properties of a small ferromagnet. Although the perpendicular spin-currents in this experiment were not very sensitive to the parameter which quantizes them, the mixing conductance $G_{\uparrow\downarrow}$, it allows to demonstrate the measurement principle. The theory described here can also be used on lateral devices which include tunnel junctions, which increases the efficiency of spin-transfer torque. In principle, the technique can also be used to study how the magnetization dynamics of spin waves are influenced by spin-transfer torque. However, the efficiency of this

[13] See also chapter 5, Fig. 5.5

process would have to be optimized to make such an effect measurable. This can be done for example by constructing multi-terminal pillar structures. In the remainder, we have proposed the aimed thermal detection of ferromagnetic resonance of a nanoscale magnet using an on-chip thermocouple. While the signals are not very large, a finite-element calculation shows that by using existing fabrication techniques it is possible to measure the generated heat with a thermocouple which is not electrically connected. By default, such a technique excludes any rectification effects which can disturb sensitive measurements[3]. We note that this measurement technique can be greatly enhanced by patterning semiconductors, of which the thermoelectric coefficients can be >100 times larger[31]. It should then be possible to detect the FMR heat of even smaller-shaped ferromagnets without the need for electrical contacts.

This experiment has recently been performed for an embedded ferromagnet[32].

References

[1] J. Slonczewski, *Current-driven excitation of magnetic multilayers*, J. Magn. Magn. Mater. **159**, L1 (1996).

[2] L. Berger, *Emission of spin waves by a magnetic multilayer traversed by a current*, Phys. Rev. B **54**, 9353 (1996).

[3] M. Costache, Ph.D. thesis, University of Groningen (2007), iSBN 978-90-367-3004-4.

[4] A. Brataas, G. Bauer, and P. Kelly, *Non-collinear magnetoelectronics*, Phys. Rep. **427**, 157 (2006).

[5] Y. Tserkovnyak, A. Brataas, G. Bauer, and B. Halperin, *Nonlocal magnetization dynamics in ferromagnetic heterostructures*, Rev. Mod. Phys. **77**, 1375 (2005).

[6] M. Johnson and R. Silsbee, *Interfacial Charge-Spin Coupling: Injection and Detection of Spin Magnetization in Metals*, Phys. Rev. Lett. **55**, 1790 (1985).

[7] F. Jedema, A. Filip, and B. van Wees, *Electrical spin injection and accumulation at room temperature in an all-metal mesoscopic spin valve*, Nature **410**, 345 (2001).

[8] C. Chappert, A. Fert, and F. Nguyen van Dau, *The emergence of spin electronics in data storage*, Nature Mater. **6**, 813 (2007).

[9] J. Sun, *Spin-current interaction with a monodomain magnetic body: A model study*, Phys. Rev. B **65**, 570 (2000).

[10] S. Zhang, S. Oliver, N. Israelof, and C. Vittoria, *High-sensitivity ferromagnetic resonance measurements on micrometer-sized samples*, Appl. Phys. Lett. **70**, 2756 (1997).

[11] F. Giesen, J. Podbielski, T. Korn, M. Steiner, A. van Staa, and D. Grundler, *Hysteresis and control of ferromagnetic resonances in rings*, Appl. Phys. Lett. **86**, 112510 (2005).

[12] M. Schneider, T. Gerrits, A. Kos, and T. Silva, *Gyromagnetic damping and the role of spin-wave generation in pulsed inductive microwave magnetometry*, Appl. Phys. Lett. **87**, 072509 (2005).

[13] C. Thirion, W. Wernsdorfer, and D. Mailly, *Switching of magnetization by nonlinear resonance studied in single nanoparticles*, Nature Mat. **2**, 524 (2003).

[14] F. Jedema, Ph.D. thesis, University of Groningen (2002), iSBN 90-367-1724-8.

[15] Sladkov, M., Master's thesis (2006).

[16] Blundell, S., *Magnetism in Condensed Matter* (Oxford University Press, 2001).

[17] Kittel, C., *Introduction to Solid State Physics* (John Wiley & Sons, Inc., 1996).

[18] M. Tsoi, A. Jansen, J. Bass, W.-C. Chiang, V. Tsoi, and P. Wyder, *Generation and detection of phase-coherent current-driven magnons in magnetic multilayers*, Nature **406**, 46 (2000).

[19] S. Kiselev, J. Sankey, I. Krivorotov, N. Emley, R. Schoelkopf, R. Buhrman, and D. Ralph, *Microwave oscillations of a nanomagnet driven by a spin-polarized current*, Nature **425**, 380 (2003).

[20] I. Krivorotov, N. Emley, J. Sankey, D. Kiselev, D. Ralph, and R. Buhrman, *Time-Domain Measurements of Nanomagnet Dynamics Driven by Spin-Transfer Torques*, Science **307**, 228 (2005).

[21] S. Kaka, M. Pufall, W. Rippard, T. Silva, S. Russek, and J. Katine, *Mutual phase-locking of microwave spin torque nano-oscillators*, Nature **437**, 389 (2005).

[22] D. Houssameddine, U. Ebels, B. Delaet, B. Rodmacq, I. Firastrau, F. Ponthenier, M. Brunet, C. Thirion, J.-P. Michel, L. Prejbeanu-Buda, et al., *Spin-torque oscillator using a perpendicular polarizer and a planar free layer*, Nature Mater. **6**, 447 (2007).
[23] F. Jedema, H. Heersche, A. Filip, J. Baselmans, and B. van Wees, *Electrical detection of spin precession in a metallic mesoscopic spin valve*, Nature **416**, 713 (2002).
[24] T. Kimura, Y. Otani, T. Sato, S. Takahashi, and S. Maekawa, *Room-Temperature Reversible Spin Hall Effect*, Phys. Rev. Lett. **98**, 156601 (2007).
[25] T. Kimura, Y. Otani, and J. Hamrle, *Enhancement of spin accumulation in a nonmagnetic layer by reducing junction size*, Phys. Rev. B **73**, 132405 (2006).
[26] L. Gravier, S. Serrano-Guisan, F. Reuse, and J.-P. Ansermet, *Thermodynamic description of heat and spin transport in magnetic nanostructures*, Phys. Rev. B **73**, 024419 (2006).
[27] Cohen-Tannoudji, C. and Diu, B. and Laloë, F., *Quantum Mechanics* (John Wiley & Sons, 1977).
[28] K. Xia, P. Kelly, G. Bauer, and I. Turek, *Spin torques in ferromagnetic/normal-metal structures*, Phys. Rev. B rapid comm. **65**, 220401 (2002).
[29] F. Bakker, A. Slachter, J.-P. Adam, and B. van Wees, *Interplay of Peltier and Seebeck effects in nanoscale nonlocal spin valves*, Phys. Rev. Lett. **105**, 136601 (2010).
[30] Slachter, A., Master's thesis (2003).
[31] R. Venkatasubramanian, E. Siivola, T. Colpitts, and B. O'Quinn, *Thin-film thermoelectric devices with high room-temperature figures of merit*, Nature **413**, 597 (2001).
[32] F. Bakker, J. Flipse, A. Slachter, and B. van Wees, *Thermoelectric detection of ferromagnetic resonance of a nanoscale ferromagnet*, ArXiv:1108.1286v1 (2011).